Inorg. Chem. **2007**, *46*, 8825–8835

Seven-Coordinate Iron and Manganese Complexes with Acyclic and Rigid Pentadentate Chelates and Their Superoxide Dismutase Activity

Gao-Feng Liu,[†] Miloš Filipović,[‡] Frank W. Heinemann,[†] and Ivana Ivanović-Burmazović*,[†]

Institute for Inorganic Chemistry, University of Erlangen-Nürnberg, Egerlandstrasse 1, 91058 Erlangen, Germany, and Department of Chemistry, University of Belgrade, 11000 Belgrade, Serbia

Received June 20, 2007

The reactions of seven-coordinate $[Fe^{III}(dapsox)(H_2O)_2]ClO_4 \cdot H_2O$ (**1**), $[Fe^{II}(H_2dapsox)(H_2O)_2](NO_3)_2 \cdot H_2O$ (**2**), and $[Mn^{II}(H_2dapsox)(CH_3OH)(H_2O)](ClO_4)_2(H_2O)$ (**3**) complexes of the acyclic and rigid pentadentate H_2dapsox ligand [H_2dapsox = 2,6-diacetylpyridinebis(semioxamazide)] with superoxide have been studied spectrophotometrically, electrochemically, and by a submillisecond mixing UV/vis stopped-flow in dimethyl sulfoxide (DMSO). The same studies were performed on the seven-coordinate $[Mn^{II}(Me_2[15]pyridinaneN_5)(H_2O)_2]Cl_2 \cdot H_2O$ (**4**) complex with the flexible macrocyclic Me_2[15]pyridinaneN_5 ligand (Me_2[15]pyridinaneN_5 = *trans*-2,13-dimethyl-3,6,9,12,18-pentaazabicyclo-[12.3.1]octadeca-1(18),14,16-triene), which belongs to the class of proven superoxide dismutase (SOD) mimetics. The X-ray crystal structures of **2**–**4** were determined. All complexes possess pentagonal-bipyramidal geometry with the pentadentate ligand in the equatorial plane and solvent molecules in the axial positions. The stopped-flow experiments in DMSO (0.06% of water) reveal that all four metal complexes catalyze the fast disproportionation of superoxide under the applied experimental conditions, and the catalytic rate constants are found to be $(3.7 \pm 0.5) \times 10^6$, $(3.9 \pm 0.5) \times 10^6$, $(1.2 \pm 0.3) \times 10^7$, and $(5.3 \pm 0.8) \times 10^6$ M^{-1} s^{-1} for **1**–**4**, respectively. The cytochrome *c* McCord–Fridovich (McCF) assay in an aqueous solution at pH = 7.8 resulted in the IC_{50} values (and corresponding k_{McCF} constants) for **3** and **4**, 0.013 ± 0.001 μM ($1.9 \pm 0.2 \times 10^8$ M^{-1} s^{-1}) and 0.024 ± 0.001 μM ($1.1 \pm 0.3 \times 10^8$ M^{-1} s^{-1}), respectively. IC_{50} values from a nitroblue tetrazolium assay are found to be 6.45 ± 0.02 and 1.36 ± 0.03 μM for **1** and **4**, respectively. The data have been compared with those obtained by direct stopped-flow measurements and discussed in terms of the side reactions that occur under the conditions of indirect assays.

Introduction

Superoxide ($O_2^{\bullet -}$) is the reactive radical anion formed following a one-electron reduction of dioxygen during numerous oxidation reactions under normal conditions in both living and nonliving systems.[1] Because it is a very good reducing agent in the anionic form and a very good oxidant in the protonated form [$pK_a(HO_2) = 4.69$], superoxide is potentially dangerous for all cellular macromolecules and can generate other undesired reactive species.[1,2] Its damaging effects lead to different pathophysiological conditions that cause aging, pain, inflammatory disorders, serious neurodegenerative diseases, and multiple types of cancer.[1b,2b,3] Therefore, the concept of removing superoxide via rapid disproportionation, i.e., dismutation (eq 1), has a protective beneficial outcome in a large number of diseases caused by the overproduction of superoxide radicals.[3a,4]

$$2O_2^{\bullet -} + 2H^+ \rightarrow H_2O_2 + O_2 \qquad (1)$$

Natural superoxide dismutase (SOD) enzymes catalyze reaction (1) and in preclinical and clinical trials have shown promising therapeutic properties, although they suffer as drug

* To whom correspondence should be addressed. E-mail: ivana.ivanovic@chemie.uni-erlangen.de.
[†] University of Erlangen-Nürnberg.
[‡] University of Belgrade.

(1) (a) Fridovich, I. *J. Biol. Chem.* **1989**, *264*, 7761−7764. (b) Fridovich, I. *Ann. N.Y. Acad. Sci.* **1999**, *893*, 13−28.
(2) (a) Liochev, S. I.; Fridovich, I. *IUBMB Life* **1999**, *48*, 157−161. (b) Salvemini, D.; Muscoli, C.; Riley, D. P.; Cuzzocrea, S. *Pulm. Pharmacol. Ther.* **2002**, *15*, 439−447 and references cited therein.
(3) (a) Muscoli, C.; Cuzzocrea, S.; Riley, D. P.; Zweier, J. L.; Thiemermann, C.; Wang, Z.-Q.; Salvemini, D. *Br. J. Pharmacol.* **2003**, *140*, 445−460 and references cited therein. (b) Stadtman, E. R. *Curr. Med. Chem.* **2004**, *11*, 1105−1112.
(4) (a) Salvemini, D.; Riley, D. P.; Cuzzocrea, S. *Nat. Rev. Drug Discovery* **2002**, *1*, 367−374. (b) Cuzzocrea, S.; Thiemermann, C.; Salvemini, D. *Curr. Med. Chem.* **2004**, *11*, 1147−1162.

10.1021/ic7012039 CCC: $37.00
Published on Web 09/20/2007

Scheme 1

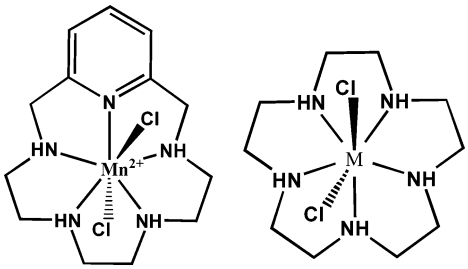

candidates primarily from immunogenic response.[2a,3a,4a,5] This calls for new types of free-radical inhibiting enzyme mimetics to be used as pharmaceuticals. Stable low molecular weight metal complexes that can react with superoxide and efficiently replicate the activity of the native SOD enzyme have the potential to become a new generation of drugs for the treatment of diseases of various aetiologies.[2b,3a,4a,5,6]

Among the many different complexes that have been studied as potential SOD mimetics,[2b,3a,5,6b,7] the most efficient synthetic SOD catalysts known to date are seven-coordinate complexes of Mn^{II} with macrocyclic pentadentate chelates derived from carbon-substituted pentaazacyclopentadecane [15]aneN_5 (Scheme 1).[2b,3a,4a,5,6a,8] Their catalytic rate constants were obtained by direct kinetic measurements, as the only reliable method for quantitative assessment of activity,[9,10] showing that the SOD activity of these complexes can exceed that of the native mitochondrial MnSOD.[6a,8g] At the same time, these complexes are the first enzyme mimetics tested in humans.

In the case of the macrocyclic Mn^{II} mimetics (Scheme 1), it has been postulated that the profound conformational rearrangements of the macrocyclic pentadentates facilitate subsequent electron transfer and that the ligands with high conformational flexibility can assist SOD activity.[8a,g] Seven-coordinate Fe^{III}SOD mimetics with the same macrocyclic chelate systems show a different catalytic mechanism in which the aqua−hydroxo form of the complex, $[Fe(L)(OH)(H_2O)]^{2+}$, is the catalytically active species.[11] A drawback of these complexes is the low-pK_a values of the two coordinated water molecules, which results in the formation of inactive (inert) dihydroxo complexes at the physiological pH.[11] Therefore, the idea is to design a chelate that will decrease the acidity of the iron center and so increase the concentration of the catalytically active aqua−hydroxo species at the physiological pH to promote an enhanced SOD activity. Because free iron ions are more toxic than manganese ions,[5] it is important that the chelate will form a very stable complex and prevent the release of iron ions. Despite this toxicity, complexes of Fe^{III} would be highly attractive as SOD mimetics because of their higher kinetic and thermodynamic stability than Mn^{II} complexes.

Because we have shown that the conformational flexibility of the pentadentate ligand is not a key requirement for the SOD activity of the seven-coordinate complexes, due to the fact that in an interchange substitution mechanism (operating in the case of these complexes)[12a] efficient formation of a real six-coordinate (with pseudo octahedral geometry) intermediate is generally not required, we were interested in additional experimental validation of such a mechanistic paradigm. This has been achieved by probing the reactivity of appropriate conformationally inflexible complexes toward superoxide.

In this paper, we have synthesized and characterized seven-coordinate Fe^{II} (**2**) and Mn^{II} (**3**) complexes of acyclic and rigid pentadentate H_2dapsox [H_2dapsox = 2,6-diacetylpyridinebis(semioxamazide)][12b] that have several important features regarding their potential SOD activity. The reactivity of these two complexes and the previously reported Fe^{III} complex (**1**) of the same ligand[12c−e] (all of which have the structure shown in Scheme 2) toward superoxide has been studied spectrophotometrically, electrochemically, and by a submillisecond mixing UV/vis stopped-flow in DMSO. The

(5) Riley, D. P. *Chem. Rev.* **1999**, *99*, 2573−2587 and references cited therein.

(6) (a) Salvemini, D.; Wang, Z.-Q.; Zweier, J. L.; Samouilov, A.; Macarthur, H.; Misko, T. P.; Currie, M. G.; Cuzzocrea, S.; Sikorski, J. A.; Riley, D. P. *Science* **1999**, *286*, 304−306. (b) Vujaskovic, Z.; Batinic-Haberle, I.; Rabbani, Z. N.; Feng, Q.-F.; Kang, S. K.; Spasojevic, I.; Samulski, T. V.; Fridovich, I.; Dewhirst, M. W.; Anscher, M. S. *Free Radical Biol. Med.* **2002**, *33*, 857−863 and references cited therein. (c) Samlowski, W. E.; Petersen, R.; Cuzzocrea, S.; Macarthur, H.; Burton, D.; McGregor, J. R.; Salvemini, D. *Nat. Med.* **2003**, *9*, 750−755. (d) Okado-Matsumoto, A.; Batinic-Haberle, I.; Fridovich, I. *Free Radical Biol. Med.* **2004**, *37*, 401−410.

(7) (a) Batinic-Haberle, I.; Spasojevic, I.; Hambright, P.; Benov, L.; Crumbliss, A. L.; Fridovich, I. *Inorg. Chem.* **1999**, *38*, 4011−4022. (b) Ohtsu, H.; Shimazaki, Y.; Odani, A.; Yamauchi, O.; Mori, W.; Itoh, S.; Fukuzumi, S. *J. Am. Chem. Soc.* **2000**, *122*, 5733−5741. (c) Li, D.; Li, S.; Yang, D.; Yu, J.; Huang, J.; Li, Y.; Tang, W. *Inorg. Chem.* **2003**, *42*, 6071−6080. (d) Durackova, Z.; Labuda, J. *J. Inorg. Biochem.* **1995**, *58*, 297−303. (e) Liao, Z.; Xiang, D.; Li, D.; Mei, F.; Yun, F. *Synth. React. Inorg. Met.−Org. Chem.* **1998**, *28*, 1327−1341. (f) Spasojević, I.; Batinić-Haberle, I.; Stevens, R. D.; Hambright, P.; Thorpe, A. N.; Grodkowski, J.; Neta, P.; Fridovich, I. *Inorg. Chem.* **2001**, *40*, 726−739. (g) Yamaguchi, S.; Kumagai, A.; Funahashi, Y.; Jitsukawa, K.; Masuda, H. *Inorg. Chem.* **2003**, *42*, 7698−7700. (h) Batinić-Haberle, I.; Spasojević, I.; Stevens, R.; Hambright, D.; Neta, P.; Okado-Matsumoto, A.; Fridovich, I. *J. Chem. Soc., Dalton Trans.* **2004**, 1696−1702. (i) Shearer, J.; Long, L. M. *Inorg. Chem.* **2006**, *45*, 2358−2360. (j) Durot, S.; Lambert, F.; Renault, J.-P.; Policar, C. *Eur. J. Inorg. Chem.* **2005**, 2789−2793.

(8) (a) Riley, D. P.; Weiss, R. H. *J. Am. Chem. Soc.* **1994**, *116*, 387−388. (b) Riley, D. P.; Henke, S. L.; Lennon, P. J.; Weiss, R. H.; Neumann, W. L.; Rivers, W. J.; Aston, K. W.; Sample, K. R.; Rahman, H.; Ling, C.-S.; Shieh, J.-J.; Busch, D. H.; Szulbinski, W. *Inorg. Chem.* **1996**, *35*, 5213−5231. (c) Riley, D. P.; Lennon, P. J.; Neumann, W. L.; Weiss, R. H. *J. Am. Chem. Soc.* **1997**, *119*, 6522−6528. (d) Riley, D. P.; Henke, S. L.; Lennon, P. J.; Aston, K. *Inorg. Chem.* **1999**, *38*, 1908−1917. (e) Riley, D. P. *Adv. Supramol. Chem.* **2000**, *6*, 217−244. (f) Krämer, R. *Angew. Chem.* **2000**, *112*, 4641−4642; *Angew. Chem., Int. Ed.* **2000**, *39*, 4469−4470. (g) Aston, K.; Rath, N.; Naik, A.; Slomczynska, U.; Schall, O. F.; Riley, D. P. *Inorg. Chem.* **2001**, *40*, 1779−1789.

(9) Riley, D. P.; Rivers, W. J.; Weiss, R. H. *Anal. Biochem.* **1991**, *196*, 344−349.

(10) Weiss, R. H.; Flickinger, A. G.; Rivers, W. J.; Hardy, M. M.; Aston, K. W.; Ryanll, U. S.; Riley, D. P. *J. Biol. Chem.* **1993**, *268* (31), 23049.

(11) Zhang, D.; Busch, D. H.; Lennon, P. L.; Weiss, R. H.; Neumann, W. L.; Riley, D. P. *Inorg. Chem.* **1998**, *37*, 956−963 and references cited therein.

(12) (a) Dees, A.; Zahl, A.; Puchta, R.; van Eikema Hommes, N. J. R.; Heinemann, F. W.; Ivanovic-Burmazovic, I. *Inorg. Chem.* **2007**, *46*, 2459−2470. (b) Andjelkovic, K.; Ivanovic, I.; Prelesnik, B. V.; Leovac, V. M.; Poleti, D. *Polyhedron* **1996**, *15* (24), 4361−4366. (c) Andjelkovic, K.; Bacchi, A.; Pelizzi, G.; Jeremic, D.; Ivanovic-Burmazovic, I. *J. Coord. Chem.* **2002**, *55*, 1385−1392. (d) Ivanovic-Burmazovic, I.; Hamza, M. S. A.; van Eldik, R. *Inorg. Chem.* **2002**, *41*, 5150−5161. (e) Ivanovic-Burmazovic, I.; Hamza, M. S. A.; van Eldik, R. *Inorg. Chem.* **2006**, *45*, 1575−1584.

Scheme 2

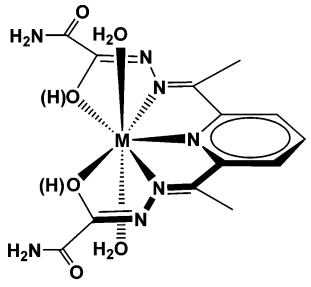

catalytic SOD activity of the complexes with the acyclic and rigid H_2dapsox ligand has been compared (under the selected experimental conditions) with the reactivity of a Mn^{II} (**4**) complex with the flexible pyridine derivative of the [15]-aneN$_5$ macrocycle (Me_2[15]pyridinaneN$_5$ = *trans*-2,13-dimethyl-3,6,9,12,18-pentaazabicyclo[12.3.1]octadeca-1(18),-14,16-triene), which belongs to the class of proven SOD mimetics.[8e] The SOD activity of the complexes has also been investigated in an aqueous solution by applying indirect cytochrome *c* and nitroblue tetrazolium (NBT) assays, and the data have been compared with those obtained by direct stopped-flow measurements and discussed in terms of the side reactions that occur under the conditions of indirect assays.

Experimental Section

Materials. All solid chemicals were of p.a. grade and used as received without any further purification. [Zn(H_2dapsox)(H_2O)$_2$]-Cl_2 used in the electrochemical measurements was synthesized according to the published procedure.[13] High-performance liquid chromatography (HPLC)-grade dimethyl sulfoxide (DMSO) containing a controlled amount of water (0.06% after mixing in a stopped-flow cuvette) was used for the complex solutions, and the water content was determined by Karl−Fischer titration. KO_2 solutions were prepared according to published procedures.[14]

Instrumentation and Measurements. Carlo Erba elemental analyzers 1106 and 1108 were used for chemical analysis. IR and UV/vis spectra were recorded on a Mattson FTIR 60 AR (KBr pellets) spectrophotometer and a Hewlett-Packard 8542A spectrophotometer, respectively.

Time-resolved UV/vis spectra were recorded on a modified Bio-Logic stopped-flow module μSFM-20 (10 ms dead time) combined with a Huber CC90 thermostat and equipped with a J&M TIDAS high-speed diode array spectrometer with a combined deuterium and tungsten lamp (200−1015 nm wavelength range). Isolast O-rings were used for all sealing purposes to enable measurements in DMSO. The spectrum of DMSO was used as a reference for all spectroscopic measurements. For the rapid kinetic measurements, the Bio-Logic stopped-flow module was upgraded to a submillisecond mixing stopped-flow configuration by combining it with a microcuvette accessory (with an optical path light of 0.8 mm) and a monochromator to minimize the dead time of the instrument. Measurements with the Fe^{II} complex were performed under an atmosphere of dry nitrogen. Data were analyzed using the integrated Bio-Kine software version 4.23 and also the Specfit/32 program. At least 10 kinetic runs were recorded under all conditions, and the reported rate constants represent the mean values.

Cyclic voltammetry measurements have been carried out using an Autolab instrument with a PGSTAT 30 potentiostat. A conventional three-electrode arrangement was employed consisting of a gold disk working electrode (geometric area: 0.07 cm^2) (Metrohm), a platinum wire auxiliary electrode (Metrohm), and the Ag(s)/AgCl-(s) wire as pseudo reference electrode, for the measurements in DMSO, or a Ag/AgCl, NaCl (3 M) (Metrohm) reference electrode, for the measurements in the aqueous solution [the potential vs NHE was calibrated by the Ag/AgCl, NaCl (3 M), potential (0.222 vs NHE)]. The measurements in DMSO were performed in the presence of 0.1 M tetrabutylammonium hexafluorophosphate as the supporting electrolyte, whereas the measurements in aqueous solutions were done by applying a 0.1 M $NaClO_4$ supporting electrolyte. All solutions without superoxide were thoroughly degassed with nitrogen prior to beginning the experiments, and during the measurements, the nitrogen atmosphere was maintained. Measurements with superoxide were carried out by saturating the solution with dry oxygen ([O_2] = 2.1 mM).[15] The sample concentration was 0.5 mM. All experiments were performed at room temperature.

Note! *It should be pointed out that for DMSO solutions only glass equipment and Hamilton Teflon valves can be used!*

Safety Notes! *Perchlorate salts of metal complexes with organic ligands are potentially explosive. Only a small amount of material should be prepared and handled with great care.*

Synthesis of [Fe^{II}(H_2dapsox)(H_2O)$_2$](NO_3)$_2$·H_2O (2). 2,6-Diacetylpyridine (0.163 g, 1 mmol) and semioxamazide (0.218 g, 2.1 mmol) were mixed in 60 mL of a methanol/acetonitrile mixture (2:1) and warmed up to 65 °C. The reaction mixture was refluxed for 2 h under an argon atmosphere. Fe(NO_3)$_3$·4H_2O (0.313 g, 1 mmol) was carefully added to the resulting white suspension, and its color changed to gray. After 1 h of refluxing, water (10 mL) was added, resulting in a clear gray solution, which was cooled down to room temperature and left standing for 5 h. The nice block crystals were filtered off, washed with a small amount of acetone, and dried in air (yield: 0.395 g, 71%). IR data (KBr, cm^{-1}): 3509s (NH), 3386s (H_2O), 3129s, 2929m, 1715s, 1677s, 1614s, 1541m (amide C═O), 1382s (amide), 1156m (CH), 822m, 681m. Anal. Calcd for $C_{13}H_{21}N_9O_{13}Fe$: C, 27.53; H, 3.73; N, 22.22. Found: C, 27.74; H, 3.12; N, 22.49.

Synthesis of [Mn^{II}(H_2dapsox)(CH_3OH)(H_2O)](ClO_4)$_2$(H_2O) (3). 2,6-Diacetylpyridine (0.163 g, 1 mmol) and semioxamazide (0.218 g, 2.1 mmol) were added to 40 mL of methanol, and the mixture was stirred at 55 °C for 1 h. Mn(ClO_4)$_2$·4H_2O (0.326 g, 1 mmol) was added into the resulting white suspension. The solution color changed to yellow, while some of the white powder still remained undissolved. The addition of 50 mL of CH_3CN resulted in a clear yellow solution. Four days later, light-yellow crystals were collected (yield: 0.393 g, 60%). IR data (KBr, cm^{-1}): 3501s (NH), 3361s (H_2O), 3247s, 1720m, 1677s, 1529m (amide C═O), 1388s (amide), 1337s, 1147m (CH) 1048w, 819m, 737m, 669m. Anal. Calcd for $C_{14}H_{23}N_7O_{15}Cl_2Mn$: C, 25.69; H, 3.54; N, 14.99. Found: C, 25.47; H, 3.24; N 14.71.

Synthesis of [Mn^{II}(Me_2[15]pyridinaneN$_5$)(H_2O)$_2$]Cl_2·H_2O (4). 3,6-Diazaoctane-1,8-diamine (1.46 g, 1.0 mmol) was added dropwise to a hot solution of $MnCl_2$·2H_2O (1.61 g, 1.0 mmol) and 2,6-diacetylpyridine (1.63 g, 1.0 mmol) in water (50 mL). After 4

(13) Sumar, M.; Ivanovic-Burmazovic, I.; Hodzic, I.; Andjelkovic, K. *Synth. React. Inorg. Met.−Org. Chem.* **2002**, *32*, 721−737.

(14) Duerr, K.; Macpherson, B. P.; Warratz, R.; Hampel, F.; Tuczek, F.; Helmreich, M.; Jux, N.; Ivanovic-Burmazovic, I. *J. Am. Chem. Soc.* **2007**, *129*, 4217−4228.

(15) Kryatov, S. V.; Rybak-Akimova, E. V.; Schindler, S. *Chem. Rev.* **2005**, *105*, 2175−2226.

Table 1. Crystal Data and Structure Refinement for **2**−**4**

	2	**3**	**4**
empirical formula	$C_{13}H_{21}N_9O_{13}Fe$	$C_{14}H_{21}Cl_2N_7O_{14}Mn$	$C_{15}H_{33}Cl_2N_5O_3Mn$
fw	567.24	637.22	457.30
cryst size (mm^3)	0.25 × 0.16 × 0.10	0.18 × 0.09 × 0.08	0.42 × 0.38 × 0.35
T (K)	100(2)	100(2)	295(2)
cryst syst	monoclinic	monoclinic	orthorhombic
space group	$P2_1/c$	$P2_1/c$	$Pbca$
a (Å)	8.0028(6)	14.632(1)	10.245(1)
b (Å)	14.6046(5)	11.257(1)	19.031(1)
c (Å)	18.226(2)	14.908(2)	22.756(1)
β (deg)	93.079(9)	99.148(6)	90
V ($Å^3$)	2127.1(3)	2424.3(4)	4436.8(5)
Z	4	4	8
F(000)	1168	1300	1928
ρ_{calcd} (Mg/m^3)	1.771	1.746	1.369
μ (mm^{-1})	0.799	0.848	0.859
reflns colld	54411	54150	9042
indep reflns	5491	5346	4521
obsd reflns [$I \geq 2\sigma(I)$]	4700	4300	2403
data/restrains/param	5491/4/388	5346/17/443	4521/ 0/318
GOF	1.034	1.059	0.986
R1 [$I \geq 2\sigma(I)$]	0.0262	0.0357	0.0520
wR2 (all data)	0.0671	0.0845	0.1189

[a] $R1 = \sum||F_o| - |F_c||/\sum|F_o|$; $wR2 = [\sum w(F_o^2 - F_c^2)^2/\sum w(F_o^2)^2]^{1/2}$.

h of refluxing, the reaction mixture was filtered and the deep-orange solution was allowed to cool down to room temperature. Deep-orange crystals of the compound $[Mn^{II}L(H_2O)_2]Cl_2$ (L = 2,13-dimethyl-3,6,9,12,18-pentaazabicyclo[12.3.1]octadeca-1(18),2,12,-14,16-pentaene) were obtained and dried under vacuum at 70 °C for 3 h (2.29 g, 69% yield). This complex (2.2 g, ca. 5 mmol) was dissolved in 40 mL of anhydrous EtOH, and the flask was flushed with argon for a few minutes. $NaBH_4$ (20 mmol, ca. 4 equiv/double bond) was added to the orange solution in one portion, and the suspension was stirred at room temperature under argon. Two hours later, the temperature was increased to 60 °C and the mixture was stirred for the next 3 h. After cooling to room temperature, the solvent was removed from the pale-yellow mixture. The residue was dissolved in water (20 mL), and NaCl (4.5 g) was added. The aqueous solution was extracted with CH_2Cl_2 (3 × 40 mL). The combined organic phases were dried ($MgSO_4$) and filtered, and the solvent was removed. The pale-yellow solid was dissolved into 5 mL of water. Colorless crystals suitable for X-ray structure analysis were obtained after 2 days (yield: 0.86 g, 18% calculated from 2,6-diacetylpyridine). IR data (KBr, cm^{-1}): 3524s (NH), 3460s, 3300s (H_2O), 3210s, 2911m, 2868s, 1628m, 1597m, 1579m (amide C═O), 1458s, 1381m (amide), 1126m, 1106s, 1009m, 1106s (CH), 1009m, 980s, 808m, 680m. Anal. Calcd for $C_{15}H_{33}Cl_2MnN_5O_3$: C, 39.40; H, 7.27; N, 15.31. Found: C, 39.38; H, 7.31; N, 15.29.

X-ray Crystal Structure Determinations. Data for **2** and **3** were collected at 100 K using a Bruker-Nonius Kappa CCD diffractometer (λ = 0.710 73 Å; graphite monochromator), while data for **4** were collected at room temperature using a Siemens P4 four-circle diffractometer (λ = 0.710 73 Å; graphite monochromator). All data sets were corrected for Lorentz and polarization effects. Absorption effects were taken into account by semiempirical methods using either multiple scans (*SADABS*)[16a] for **2** and **3** or the ψ-scan technique[16b] for **4**. The structures were solved by direct methods and refined using full-matrix least-squares procedures on F^2 (*SHELXTL NT 6.12*).[16c] The perchlorate anion in **3** is disordered; two alternative positions have been refined, resulting in occupancies of 52.0(6)% for O11−O14 and 48.0(6)% for O11′−O14′. With the exception of the hydrogen atoms of the two methyl groups in **4**, which are in calculated positions of optimized geometry, the positions of all other hydrogen atoms in **2**−**4** were derived from difference Fourier maps. The isotropic displacement parameters of all hydrogen atoms were tied to those of the equivalent isotropic displacement parameters of their corresponding carbon, nitrogen, or oxygen carrier atoms. Crystal data, data collection parameters, and refinement details of the structure determinations of complexes **2**−**4** are summarized in Table 1; selected bond distances and angles are listed in Table 2.

Indirect SOD Assays. (a) Cytochrome *c* Assay. SOD activities of complexes were measured using standard McCord−Fridovich assay[17] based on a ferricytochrome *c* reduction with superoxide produced by xanthine/xanthine oxidase. The assay was performed at 25 °C in 3 mL of a reaction buffer (50 mM potassium phosphate buffer; pH = 7.8) containing ferricytochrome *c* (10 μM), xanthine (100 μM), and an amount of xanthine oxidase such as to give a rate of $\Delta OD_{550\,nm} \approx 0.02\ min^{-1}$ (about 0.01 U mL^{-1}) in the absence of a putative SOD mimic. A reduction of ferricytochrome *c* was monitored at 550 nm. After 150 s, different amounts of the putative SOD mimic were added. Rates were linear for at least 8 min. Both rates in the absence and in the presence of the complex were determined for each concentration of complex added and plotted against it. The IC_{50} value represents the concentration of putative SOD mimic that induces a 50% inhibition of the reduction of cytochrome *c*.

(b) Reliability of the McCord−Fridovich Assay. To check that the tested compounds do not inhibit the production of superoxide by xanthine oxidase, the rate of conversion of xanthine to urate (see below) was determined by measuring the increase in the absorbance at 290 nm over a 2 min period with and without the tested compounds. To measure the rate of conversion of xanthine to urate, xanthine oxidase (20 μL of 1 U mL^{-1} XO) was added to a solution of 50 mM potassium phosphate buffer, pH = 7.8, containing xanthine (150 μM) at a final volume of 1.0 mL at 25 °C. Urate production was monitored at 290 nm.[18] No difference

(16) (a) *SADABS*, version 2.06; Bruker AXS, Inc.: Madison, WI, 2002. (b) North, A. C. T.; Phillips, D. C.; Mathews, F. S. *Acta Crystallogr.* **1968**, *A24*, 351−359. (c) *SHELXTL NT 6.12*; Bruker AXS, Inc.: Madison, WI, 2002.

(17) McCord, J. M.; Fridovich, I. *J. Biol. Chem.* **1969**, *244*, 6049−6055.

Table 2. Selected Bond Distances (Å) and Angles (deg) for **2**−**4**

		Compound **2**	
Fe1−O5	2.144(1)	Fe1−O6	2.159(1)
Fe1−O1	2.179(1)	Fe1−O3	2.195(1)
Fe1−N1	2.206(2)	Fe1−N2	2.233(2)
Fe1−N5	2.218(2)		
O3−C12	1.232(2)	O1−C8	1.234(2)
N6−C12	1.343(2)	N3−C8	1.346(2)
N2−N3	1.375(2)	N2−C6	1.289(2)
N5−N6	1.372(2)	N5−C10	1.287(2)
O5−Fe1−O6	178.88(4)	O5−Fe1−N5	91.96(4)
O5−Fe1−O1	88.10(4)	O6−Fe1−N5	87.04(4)
O6−Fe1−O1	93.01(4)	O1−Fe1−N5	148.91(4)
O5−Fe1−O3	91.79(4)	O3−Fe1−N5	71.80(4)
O6−Fe1−O3	88.37(4)	N1−Fe1−N5	70.15(4)
O1−Fe1−O3	77.12(3)	O5−Fe1−N2	88.53(4)
O5−Fe1−N1	90.03(4)	O6−Fe1−N2	91.92(4)
O6−Fe1−N1	89.16(4)	O1−Fe1−N2	71.14(4)
O1−Fe1−N1	140.93(4)	O3−Fe1−N2	148.23(4)
O3−Fe1−N1	141.95(4)	N1−Fe1−N2	69.80(4)
N5−Fe1−N2	139.95(4)		
		Compound **3**	
Mn1−O5	2.152(2)	Mn1−N1	2.287(2)
Mn1−O6	2.192(2)	Mn1−N2	2.306(2)
Mn1−O1	2.224(4)	Mn1−O3	2.359(2)
Mn1−N5	2.281(2)		
O1−C8	1.242(3)	O3−C12	1.227(3)
N2−C6	1.283(3)	N5−C10	1.281(3)
N2−N3	1.379(2)	N5−N6	1.371(2)
N3−C8	1.338(3)	N6−C12	1.347(3)
O5−Mn1−O6	171.94(7)	N5−Mn1−N1	68.09(6)
O5−Mn1−O1	91.62(6)	O5−Mn1−N2	95.90(7)
O6−Mn1−O1	90.87(6)	O6−Mn1−N2	92.16(6)
O5−Mn1−N5	87.48(7)	O1−Mn1−N2	69.78(6)
O6−Mn1−N5	86.89(6)	N5−Mn1−N2	136.46(6)
O1−Mn1−N5	153.70(6)	N1−Mn1−N2	68.39(6)
O5−Mn1−N1	93.00(7)	O5−Mn1−O3	87.57(6)
O6−Mn1−N1	90.25(7)	O6−Mn1−O3	85.05(6)
O1−Mn1−N1	138.17(6)	O1−Mn1−O3	84.31(5)
N5−Mn1−O3	69.40(6)		
		Compound **4**	
Mn1−O2	2.241(3)	Mn1−N3	2.330(4)
Mn1−N1	2.278(3)	Mn1−N2	2.343(3)
Mn1−O1	2.282(3)	Mn1−N5	2.352(3)
Mn1−N4	2.320(3)		
O2−Mn1−N1	89.0(2)	O2−Mn1−N2	86.0(2)
O2−Mn1−O1	173.4(2)	N1−Mn1−N2	70.2(2)
N1−Mn1−O1	85.3(2)	O1−Mn1−N2	89.0(2)
O2−Mn1−N4	83.7(2)	N4−Mn1−N2	145.2(2)
N1−Mn1−N4	142.4(2)	N3−Mn1−N2	74.7(2)
O1−Mn1−N4	102.9(2)	O2−Mn1−N5	95.0(2)
O2−Mn1−N3	99.1(2)	N1−Mn1−N5	70.3(2)
N1−Mn1−N3	143.3(2)	O1−Mn1−N5	86.2(2)
O1−Mn1−N3	83.6(2)	N4−Mn1−N5	73.7(2)
N4−Mn1−N3	74.3(2)	N3−Mn1−N5	143.2(2)
N2−Mn1−N5	140.5(2)		

in the slope was recorded with or without the putative SOD mimics. To exclude the possibility of hydrogen peroxide interference with the assay[10] and with the intent to avoid catalase addition (which can make the system more complex), catalase activity of complexes was monitored as described previously.[18] No catalase-type activity of our complexes was detected.

(c) Modified NBT Assay. To further probe SOD activity of our complexes, a modified NBT assay was used.[7i,19a] In this essay, an extensive excess of superoxide against catalyst was used. A total of 1 mg of solid KO_2 was added into 2 mL of 50 mM potassium phosphate buffer, pH = 7.8, containing putative SOD mimetic, and after 2 min, spectra were recorded. NBT reacted with superoxide, forming blue pigment formazan [$\lambda_{max} \approx 580$ nm (35 000 M^{-1} cm^{-1})].[19b] The presence of the complex caused concentration-dependent inhibition of formazan formation, as followed by the absorbance change at 580 nm. The concentration that causes 50% of the formazan formation was indicated as IC_{50}.

(18) Policar, C.; Durot, S.; Lambert, F.; Cesario, M.; Ramiandrasoa, F.; Morgenstern-Badarau, I. *Eur. J. Inorg. Chem.* **2001**, 1807−1818.

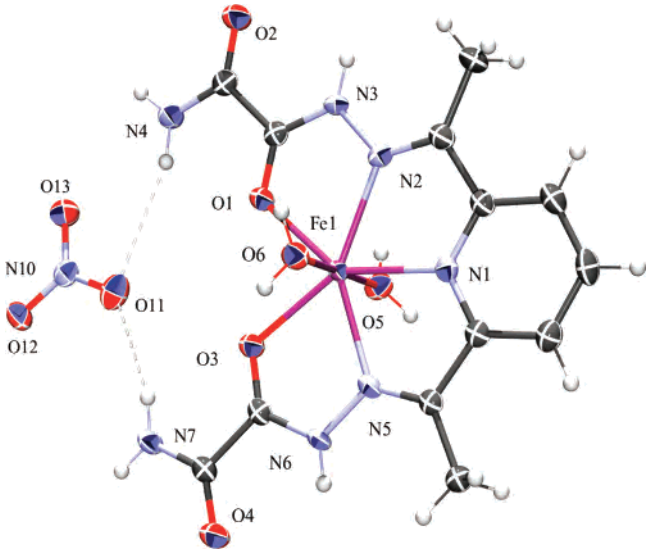

Figure 1. ORTEP view of $[Fe^{II}(H_2dapta)(H_2O)_2(NO_3)]^+$ in the crystal of **2** drawn with thermal ellipsoids at 50% probability level. Another nitride anion is omitted for clarity.

Results and Discussion

Structures. The cationic $[Fe^{II}(H_2dapsox)(H_2O)_2]^{2+}$ complex (**2**; Figure 1) has a pentagonal-bipyramidal (PBP) structure with a neutral pentadentate H_2dapsox ligand in the equatorial plane and two water molecules in axial positions. H_2dapsox is coordinated to the Fe^{II} center through the pyridine nitrogen, two imine nitrogen atoms, and two oxygen atoms of hydrazide C═O groups. These five donor atoms are almost perfectly coplanar, and the mean deviation from planarity is just 0.0137 Å. The central Fe^{II} ion is only 0.0034(5) Å below this plane. The sum of four chelate angles and the bite O1−Fe1−O3 angle (Table 2) is 360.01°, very close to 360° for an ideal planar structure. Two axial water molecules (O5 and O6) complete PBP, forming an almost linear angle [O5−Fe1−O6 = 178.88(4)°]. The intraligand bond lengths (Table 2) suggest that the neutral H_2dapsox ligand is coordinated to the Fe^{II} center in a hydrazide >C═N−NH−C═O form, different from the α-oxiazine >C═N−N═C−O^- form of the deprotonated $dapsox^{2-}$ ligand present in the PBP structure of the corresponding Fe^{III} ($[Fe^{III}(dapsox)(H_2O)_2]^+$) complex.[12c] In the Fe^{II} complex, the average C−N distance is a bit longer (1.316 Å), whereas the average C−O (1.233 Å) and N−N (1.374 Å) distances are shorter than those found in the Fe^{III} complex (1.296, 1.280, and 1.392 Å, respectively). Despite the change in the metal-ion size and ligand charge, there is just a small increase

(19) (a) Dutta, S.; Padhye, S.; Ahmed, F.; Sarkar, F. *Inorg. Chim. Acta* **2005**, *358*, 3617−3624. (b) Bielski, B. H. J.; Shiue, G. G.; Bajuk, S. *J. Phys. Chem.* **1980**, *84*, 830.

in the average Fe−N equatorial bond length from the Fe^{III} complex to the corresponding Fe^{II} complex (ca. 0.022 Å). The same was observed in the case of the macrocyclic iron PBP complexes, where the small effect was explained in terms of the rigid nature of the cyclic ligands.[20] However, the acyclic nature of our ligand suggests that the weak sensitivity of the Fe−N bonds to the change in the metal oxidation state is a more general feature of the unsaturated segments of the pentadentate ligands. From another side, the average Fe−O equatorial bond length is significantly longer in the Fe^{II} (2.187 Å) complex than in the Fe^{III} (2.056 Å) complex. The negative charge of the coordinated α-oxiazine oxygen atoms additionally strengths the Fe^{III}−O bond. The prominent elongation of the average Fe−OH_2 bond length from the Fe^{III} complex (2.028 Å) to the Fe^{II} complex (2.152 Å) is observed, confirming that the axial distances reflect changes in the ion size more readily than the equatorial ones.[21] Interestingly, the asymmetry in the two Fe−N(imine) bonds in $[Fe^{II}(H_2dapsox)(H_2O)_2]^{2+}$ (0.015 Å) is somewhat more prominent than that in $[Fe^{III}(dapsox)(H_2O)_2]^{+}$ (0.007 Å). However, it is ca. 2 times smaller than that in the case of the very similar $[Fe^{II}(H_2dapsc)(H_2O)(Cl)]^{+}$ complex (0.034 Å), where the difference in these two bonds was rationalized in terms of the high-spin d^6 configuration and the Jahn−Teller effect in a PBP field.[21] The differences in the two equatorial Fe−O bonds are identical (ca. 0.02 Å) in all three structures ($[Fe^{III}(dapsox)(H_2O)_2]^{+}$, $[Fe^{II}(H_2dapsox)(H_2O)_2]^{2+}$, and $[Fe^{II}(H_2dapsc)(H_2O)(Cl)]^{+}$) and are not affected by the change in the iron oxidation state and charge of the oxygen atom. The average Fe−N and Fe−O equatorial bonds in $[Fe^{II}(H_2dapsox)(H_2O)_2]^{2+}$ and $[Fe^{II}(H_2dapsc)(H_2O)(Cl)]^{+}$ are almost identical. Even more, the average Fe−OH_2 bond length in $[Fe^{II}(H_2dapsox)(H_2O)_2]^{2+}$ and the corresponding bond length in $[Fe^{II}(H_2dapsc)(H_2O)(Cl)]^{+}$ are also identical. This shows that the axial coordination of Cl^- does not affect the bonds either in the equatorial plane or in its trans position.

The two terminal −NH_2 groups are involved in intramolecular hydrogen bonds with the metal-coordinated hydrazide oxygen atoms [N4−H···O1 2.666(2) Å and N7−H···O3 2.714(2) Å; given are only the donor−acceptor distances for the hydrogen bridges discussed, and complete details can be found in Table S1 in the Supporting Information], similar to those observed in the structure of $[Fe^{III}(dapsox)(H_2O)_2]^{+}$.[12c] The presence of the hydrogen atom on the hydrazide nitrogen enables the formation of additional intramolecular hydrogen bonds between the hydrazide nitrogen atoms N6 or N3 and the amide oxygen atoms O2 and O4 [N3−H···O2 2.793(2) Å and N6−H···O4 2.692(2) Å]. Although hydrogen-bond interaction between the cationic complex and the NO_3^- counteranion is observed [N7−H···O11 3.002(2) Å and N4−H···O11 3.486(2) Å], the ion-pair association in this structure is not as prominent as it is in the case of the interactions between ClO_4^- and $[Fe^{III}(dapsox)(H_2O)_2]^{+}$, where ClO_4^- participates in an extensive hydrogen-bond network. Interestingly, this interaction between ClO_4^- and amide tails of the tweezer-like cationic complex is even observed in the MeCN solution of the Fe^{III} as well as the Fe^{III} form of the complex.[22]

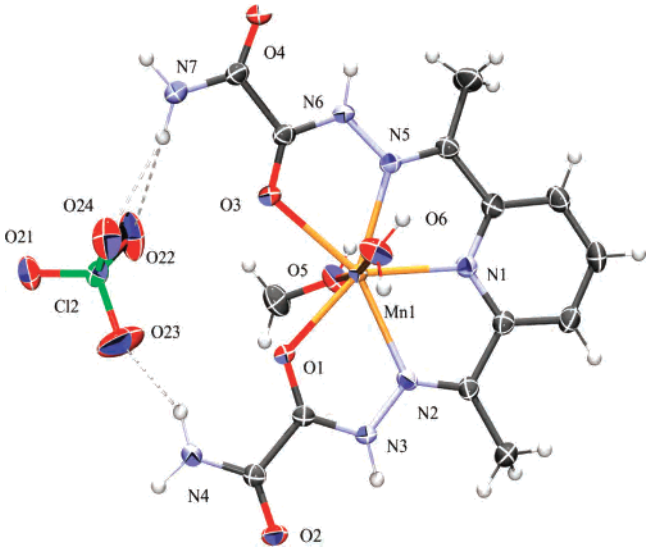

Figure 2. ORTEP view of $[Mn^{II}(H_2dapsox)(H_2O)(CH_3OH)(ClO_4)]^{+}$ in the crystal of **3** drawn with thermal ellipsoids at 55% probability level. Another perchloride anion is omitted for clarity.

The $[Mn^{II}(H_2dapsox)(CH_3OH)(H_2O)]^{2+}$ complex (**3**; Figure 2) also has the PBP structure with the neutral pentadentate ligand coordinated in the equatorial plane in a hydrazide >C═N−NH−C═O form. Thus, the intraligand bond lengths are almost identical with those in the above-discussed Fe^{II} complex (Table 2). However, the Mn−N and Mn−O bonds are all longer than the corresponding Fe−N and Fe−O bonds (Table 2). The sum of the chelate angles and the bite angle is 359.97°, which means that the five donor atoms from H_2-dapsox form an ideal planar structure. In fact, the mean deviation of this plane is just 0.0195 Å, with the central Mn^{II} ion a little below this plane [the distance from the plane is ca. 0.0412(8) Å].

In comparison with the similar structure of $[Mn^{II}(H_2dapsc)(H_2O)(Cl)]^{+}$,[21] it can be seen that, even though the average Mn−N bond length is the same for both structures (ca. 2.291 Å), the average Mn−O equatorial bond length is significantly longer in our complex (2.291 vs 2.216 Å), showing that there is no general interrelation between the equatorial distances, as was suggested. Even more, the difference between two Mn−O equatorial bond lengths is very significant (0.135 Å), although such a distortion is not expected for the spherically symmetrical high-spin d^5 electronic configuration. This shows that the intra- and intermolecular secondary interactions within the crystal packing have an important influence on the symmetry of the coordination sphere. As in the case of **2**, the intramolecular hydrogen bonds are observed between terminal −NH_2 groups and the corresponding metal-coordinated hydrazide oxygen atoms [N4−H···O1 2.703(2) Å and N7−H···O3 2.763(2) Å] and between the hydrazide nitrogen and amide oxygen atoms [N3−H···O2 2.749(2) Å and N6−H···O4 2.630(2) Å]. As mentioned above, an

(20) Drew, M. G. B.; Hamid bin, O. A.; Nelson, S. M. *J. Chem. Soc., Dalton Trans.* **1976**, 1394.
(21) Palenik, G. J.; Wester, D. W. *Inorg. Chem.* **1978**, *17*, 864−870.
(22) Sarauli, D.; Popova, V.; Zahl, A.; Puchta, R.; Ivanović-Burmazović, I. *Inorg. Chem.* **2007**, in press.

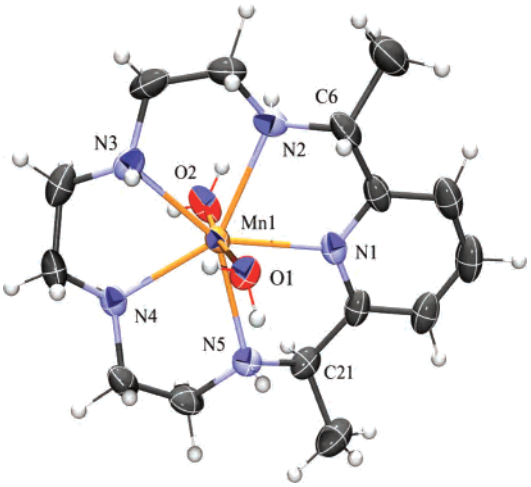

Figure 3. ORTEP view of $[Mn^{II}(Me_2[15]pyridinaneN_5)(H_2O)_2]^{2+}$ in the crystal of **4** drawn with thermal ellipsoids at 25% probability level. The chloride anion is omitted for clarity.

Scheme 3

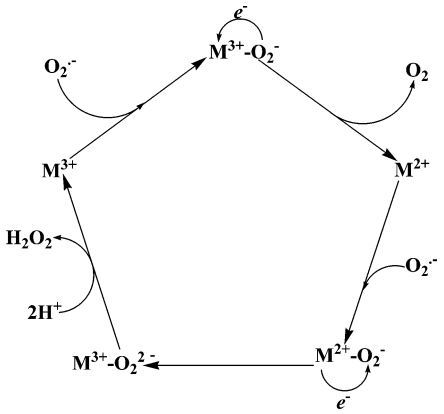

interesting feature of the tweezer-like complexes of H_2dapsox is their association with the anion by means of shape recognition, hydrogen-bond complementarity, and charge assistance. The perchlorate anion is chelated by the cationic $[Mn^{II}(H_2dapsox)(CH_3OH)(H_2O)]^{2+}$ complex via hydrogen bonds [N4−H···O23 2.924(3) Å, N7−H···O24 3.136(3) Å, and N7−H···O22 3.578(3) Å], closing the cavity of the complex and forming sort of a macrocyclic structure.

In order to compare the reactivity of our complexes with that of a proven SOD catalyst under the selected experimental conditions, we have synthesized and characterized the $[Mn^{II}(Me_2[15]pyridinaneN_5)(H_2O)_2]^{2+}$ complex (**4**) with the flexible pyridine derivative of the [15]aneN$_5$ macrocycle, which belongs to the class of proven SOD mimetics.[8] Similar to other [Mn([15]aneN$_5$)]-type complexes,[8e,g] $[Mn^{II}(Me_2[15]pyridinaneN_5)(H_2O)_2]^{2+}$ exists in the seven-coordinate PBP geometry but crystallizes as a *trans*-diaqua complex instead of a *trans*-dichloro complex. The Mn−N bond distances and angles (Figure 3) are all quite similar to those observed for other complexes of the same class. **4** crystallizes as a mixture of (*S*,*S*)- and (*R*,*R*)-dimethyl enantiomers with a C−CH$_3$ and N−H pattern on the macrocycle, which alternates as up−down−up−down. Consequently, the two sides of the macrocyclic plane and the two axial coordination sites as well are chemically equivalent. By way of comparison with the

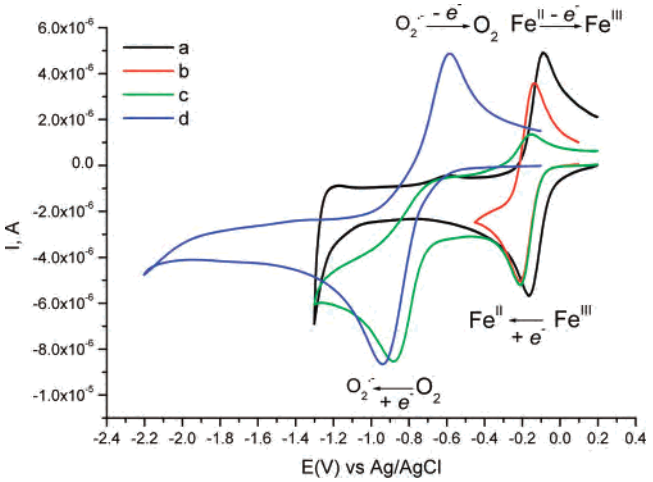

Figure 4. Cyclic voltammogramms of (a) **1** purged with nitrogen, (b) **1** purged with dioxygen, (c) **1** purged with dioxygen, and (d) pure DMSO purged with dioxygen. Conditions: [complex] = 0.5 × 10^{-3} M; [Bu_4NBF_4] = 0.1 M; T = 298 K; scan rates = 0.2 V s^{-1}.

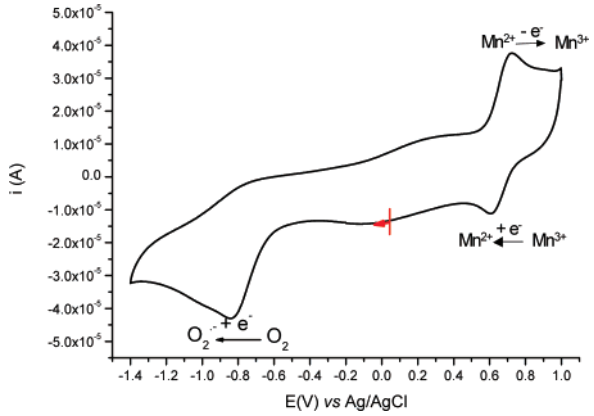

Figure 5. Cyclic voltammogramm of **3** purged with dioxygen. Conditions: [**3**] = 0.5 × 10^{-3} M; [Bu_4NBF_4] = 0.1 M; T = 298 K, in a DMSO solution; scan rates = 0.2 V s^{-1}.

analogous imine groups containing complex,[23] the average Mn−N distance in **4** is somewhat longer because the double-bond-containing ligand has a smaller cavity. The structure of the Fe^{III} complex with the same ligand is known,[24] but the ligand is present in its (*R*,*S*)-dimethyl diastereomer form where two methyl groups are on the same side of the FeN$_5$ plane.

Electrochemistry. The metal-centered redox potential is the most important criterion for the complex to be a SOD mimetic because the catalytic disproportionation of $O_2^{\bullet-}$ requires redox reactions between the complex and superoxide (Scheme 3). The complex redox potential should fall between the redox potentials for the reduction and oxidation of $O_2^{\bullet-}$, viz. −0.16 and +0.89 V vs NHE, respectively.[25]

Aqueous solutions of $[Fe(dapsox)(H_2O)_2]ClO_4$ (**1**) in the pH range of 1−12 exhibit a reversible redox wave for the Fe^{III}/Fe^{II} couple, and no complex decomposition or dimerization was observed.[26] Furthermore, in the pH range of 1−10, the metal-centered redox potential for [Fe(dapsox)-

(23) Omar, J.-S.; Daniel, R.-R.; del María, J. R.-H.; Martha, E. S.-T.; Rafael, Z.-U. *J. Chem. Soc., Dalton Trans.* **1998**, 1551−1556.
(24) Drew, M. G. B.; Rice, D. A.; Silong, S. B. *Polyhedron* **1983**, *2*, 1053−1056.

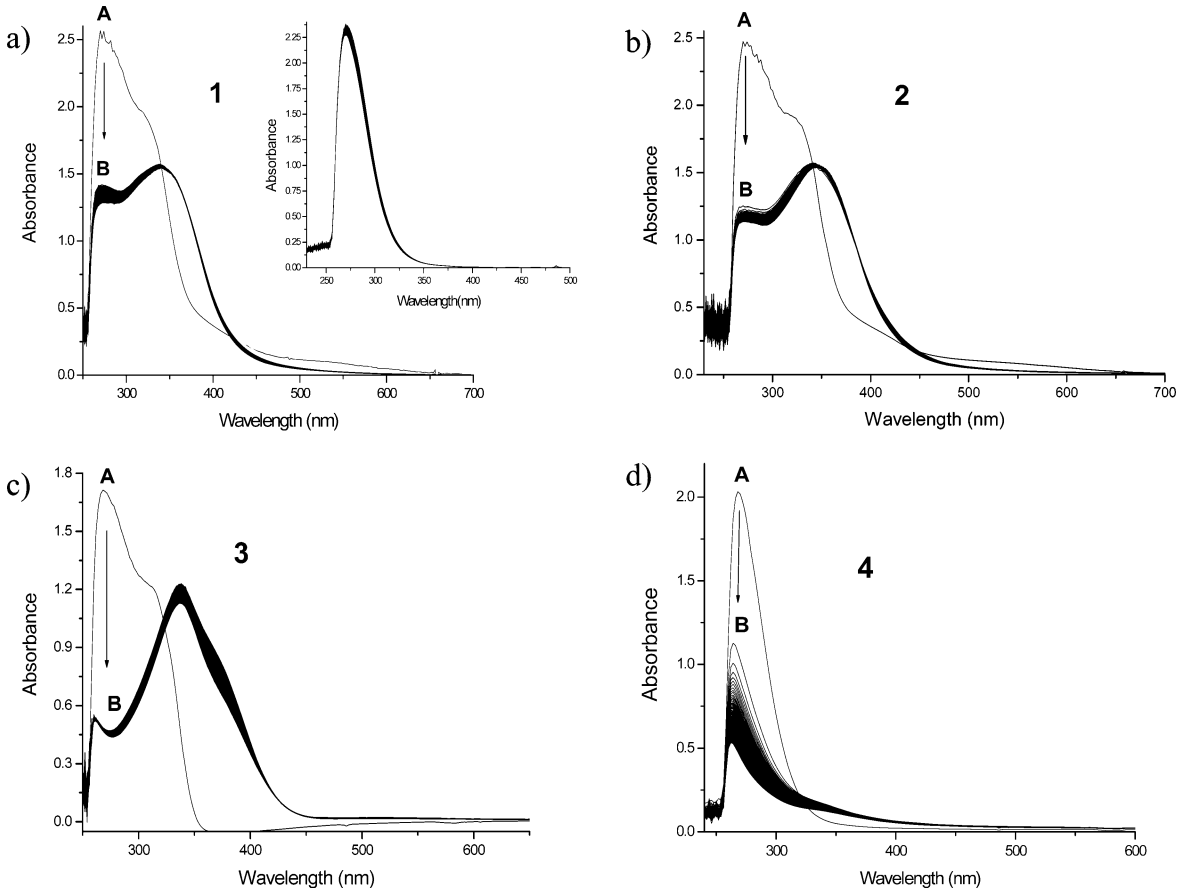

Figure 6. Time-resolved UV/vis spectra recorded for the reaction of a 5×10^{-5} M complex with 1 mM KO_2 in DMSO at room temperature for **1** (a), **2** (b), **3** (c), and **4** (d). A: spectrum recorded (measurements in a tandem cuvette) before mixing. B: first spectrum obtained after mixing (using a stopped-flow module) followed by spectra recorded at time intervals of 10 s (total observation time 2.5 h). Inset: control reaction without the addition of the complex followed over 2.5 h.

$(H_2O)_2]ClO_4$ is in the range required for the possible SOD activity. For the Fe^{III} complexes with [15]aneN_5 types of chelates that are proven SOD catalysts, the redox potentials were not reported for the physiological pH, at which these complexes exist as an equilibrium mixture of the dihydroxo and aqua−hydroxo species.[11] At pH ∼ 3, they have redox potentials in the range of 0.35−0.45 V vs NHE. In comparison, our complex at pH = 3 and 7.8 shows reversible redox behavior at 0.34 and 0.05 V vs NHE, respectively. It should be noted that dapsox^{2-} causes an increase in the pK_a values of the coordinated water molecules (pK_{a1} = 5.8 and pK_{a2} = 9.5),[12d,26] which are very close to those of the native Fe^{III}SOD enzyme (∼5 and ∼9).[27] Thus, at the physiological pH, almost 100% of the complex is in the catalytically active aqua−hydroxo form.

The cyclic voltammogram for **1** in DMSO purged with nitrogen exhibits a reversible couple at −0.13 V vs Ag/AgCl electrode (Figure 4a), or −0.11 vs NHE, obtained by calibration with ferrocene. The cyclic voltammogram in dioxygen-saturated DMSO in the scan range up to −0.4 V (Figure 4b) shows again a reversible redox wave for the Fe^{III}/Fe^{II} couple at slightly more negative potential, −0.18 V, because in the presence of oxygen, it is more difficult to reduce Fe^{III}. When the scan proceeds toward more negative potentials (Figure 4c), after the complex is reduced to the Fe^{II} species, molecular oxygen is reduced to superoxide at −0.82 V. When the scan is then returned to 0.2 V, no corresponding anodic peak assigned to the oxidation of $O_2^{\bullet-}$ is found, in contrast to the reversible redox behavior for dioxygen in DMSO solutions (Figure 4d). The intensity of the anodic peak corresponding to the oxidation of Fe^{II} is also significantly decreased. This suggests that the iron complex (starting from the electrochemically generated Fe^{II} form) catalytically decomposes superoxide (the Fe^{II} form, present in lower concentration than $O_2^{\bullet-}$, consumes all of it). The superoxide decomposition is also observed by applying much lower (catalytic) concentrations of the complex (Figure S1 in the Supporting Information).

Similar to the proven seven-coordinate Mn^{II}SOD mimetics with [15]aneN_5 types of chelates,[8b] **3** is stable in the pH range of 6−10.5 and in methanol exhibits a reversible redox potential at 0.8 V vs NHE.[8a,b] The redox behavior in aqueous solutions for the macrocyclic MnSOD mimetics was not reported. We measured the cyclic voltammograms for **4** (E_{ox} = 0.98 V and E_{red} = 0.35 V) and **3** (E_{ox} = 0.64 V and E_{red} = 0.20 V) at pH = 7.8, and both complexes show similar

(25) Stanbury, D. M. *Adv. Inorg. Chem.* **1989**, *33*, 70−138.
(26) Sarauli, D.; Meier, R.; Liu, G.-F.; Ivanovic-Burmazovic, I.; van Eldik, R. *Inorg. Chem.* **2005**, *44*, 7624−7633.
(27) Lah, M. S.; Dixon, M. M.; Pattridge, K. A.; Stallings, W. C.; Fee, J. A.; Ludwig, M. L. *Biochemistry* **1995**, *34*, 1646−1660.

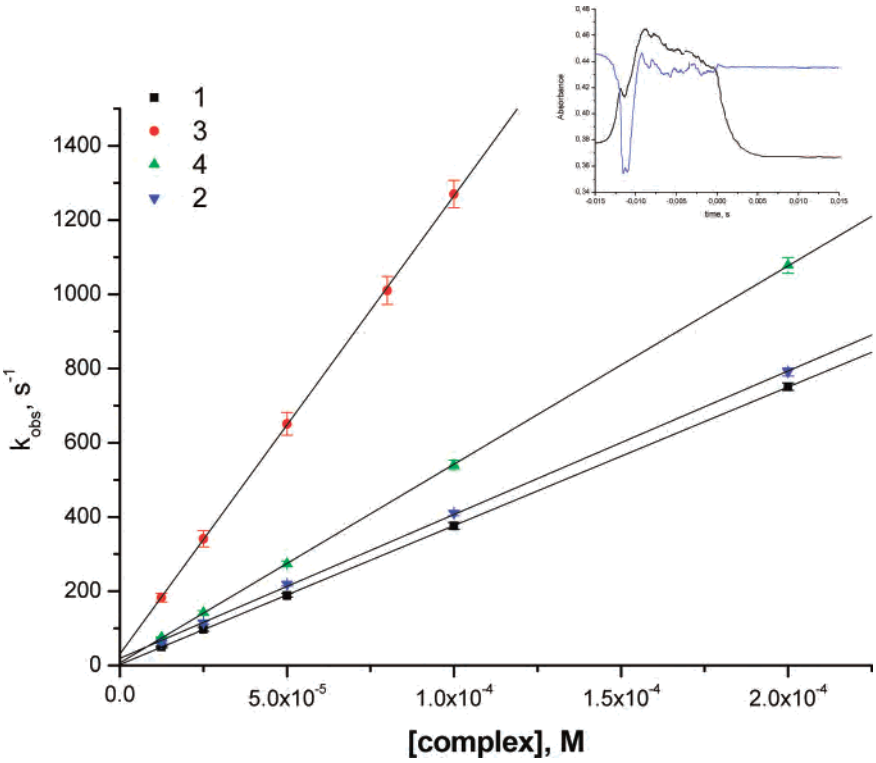

Figure 7. Plots of k_{obs} vs [complex] for the reaction between complexes and saturated KO_2 in a DMSO solution at room temperature. Inset: kinetic trace for [**1**] = 2×10^{-4} M and control reaction without the addition of the complex obtained by using submillisecond mixing stopped-flow configuration.

behavior with large peak separation (Figure S2 in the Supporting Information).

Electrochemical measurements in dioxygen-saturated DMSO (Figure 5) show, as in the case of **1**, that **3** can also catalytically decompose superoxide (disappearance of the anodic peak assigned to the oxidation of $O_2^{\bullet-}$ in the presence of the Mn^{II} form of the complex), remaining unchanged (appearance of a reversible redox wave for the Mn^{II}/Mn^{III} couple at 0.65 V). In comparison, the proven SOD mimetic **4** upon reaction with superoxide undergoes modification, and in the scan range from 0 to 1.2 V and back to 0 V, three oxidation and reduction peaks appear (Figure S3 in the Supporting Information).

Control electrochemical measurements of the $[Zn(H_2dapsox)(H_2O)_2]^{2+}$ complex in nitrogen- and dioxygen-saturated DMSO confirmed that H_2dapsox was not the redox-active ligand (the zinc complex is electrochemically silent) and that in the presence of its non-redox-active metal complex electrochemically generated superoxide was stable (the anodic peak assigned to the oxidation of $O_2^{\bullet-}$ does not disappear in the presence of the zinc complex).

Reaction with Superoxide in DMSO. We studied the reactions of **1**−**4** (Figure 6), with a large excess of $O_2^{\bullet-}$ in DMSO containing a controlled amount of water (0.06%), which was in excess over the superoxide and complex concentrations. Water present in the DMSO solution plays an important role and enables the catalytic decomposition of $O_2^{\bullet-}$. Similar to what was reported in the literature,[8a] under absolute water-free conditions only a stoichiometric reaction between $O_2^{\bullet-}$ and the complex could be observed and the catalytic process was suppressed. Time-resolved UV/vis spectra (Figure 6) show that immediately after mixing of a superoxide solution with a complex solution, rapid decomposition of $O_2^{\bullet-}$ (decrease in the absorbance in the 240−330 nm range within the dead time of the stopped-flow instrument) was observed. The products of superoxide disproportionation, O_2 and H_2O_2, were qualitatively detected in all four experiments.[28] In the case of **4**, following fast superoxide decomposition, the complex starts to decompose slowly and results in the formation of a light-brown colloid precipitate (presumably MnO_2) after ∼3 h. Three hours after mixing with KO_2, acid was added to the solutions of complexes **1**−**3**, which resulted in the recovery of the initial **1** and **3** complexes, respectively. This demonstrates that our acyclic complexes are more stable than the macrocyclic complex **4** under the applied experimental conditions, which is in agreement with the electrochemical observations (see above).

The rapid process was quantified by following the corresponding absorbance decrease at 270 nm in a series of stopped-flow measurements, in which the catalytic concentration of the studied complexes was varied. Application of a microcuvette accessory (which reduced the dead time of the instrument down to 0.4 ms) enabled observation of the fast disappearance of the 270 nm absorption, which could best be fitted as a first-order process to obtain the characteristic k_{obs} (s^{-1}) value. When experiments were performed using the complex solutions with a higher amount of water,

(28) For the O_2 detection, see: Karlin, K. D.; Cruse, R. W.; Gultneh, Y.; Farooq, A.; Hayes, J. C.; Zubieta, J. *J. Am. Chem. Soc.* **1987**, *109*, 2668−2679. For the H_2O_2 detection, a peroxide indicator paper suitable for the organic solvents (QUANTOFIX-Peroxide 100) was used.

Table 3. Catalytic Rate Constants and IC_{50} Values Obtained by Using Direct Stopped-Flow Measurements in DMSO (0.06% Water) and an Indirect Cytochrome *c* Assay in an Aqueous Solution (Phosphate Buffer pH = 7.8), Respectively

complex	$k_{cat.}$ (M^{-1} s^{-1})	IC_{50} (μM)	k_{McCF} (M^{-1} s^{-1})
MnSOD		0.005 ± 0.001	$5.2 \pm 0.2 \times 10^8$
1	$(3.7 \pm 0.5) \times 10^6$		
2	$(3.9 \pm 0.5) \times 10^6$		
3	$(1.2 \pm 0.3) \times 10^7$	0.013 ± 0.001	$1.9 \pm 0.2 \times 10^8$
4[a]	$(5.3 \pm 0.8) \times 10^6$	0.024 ± 0.001	$1.1 \pm 0.3 \times 10^8$

[a] $k_{cat.} = 1.0 \times 10^7$ M^{-1} s^{-1} was obtained in an stopped-flow experiment with $DMSO/H_2O = 1/18$.[8a−d,9]

it was not possible to quantify the corresponding rate constants because the higher water contents caused a mixing problem on a short time scale. In Figure 7, the obtained k_{obs} values are reported as a function of the complex concentration for our iron and manganese complexes, as well as for the proven SOD mimetic. A good linear correlation between k_{obs} and the complex concentration was observed for all studied complexes. From the slope of the plot of k_{obs} vs catalyst concentration, the catalytic rate constants ($k_{cat.}$)[9,10] were determined (Table 3). The $k_{cat.}$ values show that both iron complexes and the macrocyclic manganese complex have almost the same catalytic activity, within the error limits, whereas **3** has approximately 2 times higher activity. It should be stressed that it does not matter whether the Fe^{III} or Fe^{II} form of the complex is used; identical spectral changes (Figure 6) and kinetic behavior (Figure 7) are observed upon reaction with superoxide, which is consistent with the redox cycling of the complex during $O_2^{\bullet -}$ decomposition (Scheme 3).

Reaction with Superoxide in Aqueous Solutions. To prove the reactivity of our complexes toward superoxide in an aqueous buffer, a McCord−Fridovich assay (here referred to as a X/XO assay)[17] and modified NBT[7i,19a] assays were used.

The X/XO assay is based on kinetic competition for the superoxide reaction between oxidized cytochrome *c* and the complex showing SOD activity. The reduction of ferricytochrome *c* was followed spectrophotometrically at 550 nm. Both **3** and **4** were found to inhibit the reduction of cytochrome *c* when injected into the solution, as shown in Figure 8a. Inhibition percentages were measured for several complex concentrations (Figure 8b), and IC_{50} values, calculated using the graphical method, are reported in Table. 3. Although used as a feature characterizing the SOD activity of the complex, IC_{50} values strongly depend on the concentration of the detector used and are thus not appropriate for comparison with the literature.[18] From the measured IC_{50} values, it is possible to calculate a catalytic constant (k_{McCF}), which is independent of the detector concentration. At the IC_{50} concentration, superoxide reacts at the same rate with the detector and with the putative SOD mimic. Then, $k_{McCF} = k_{detector}[detector]/IC_{50}$.[29] Upon a comparison of the obtained k_{McCF} constants with those found in the literature,[6,18,30] **3** belongs to the very active SOD mimetics.

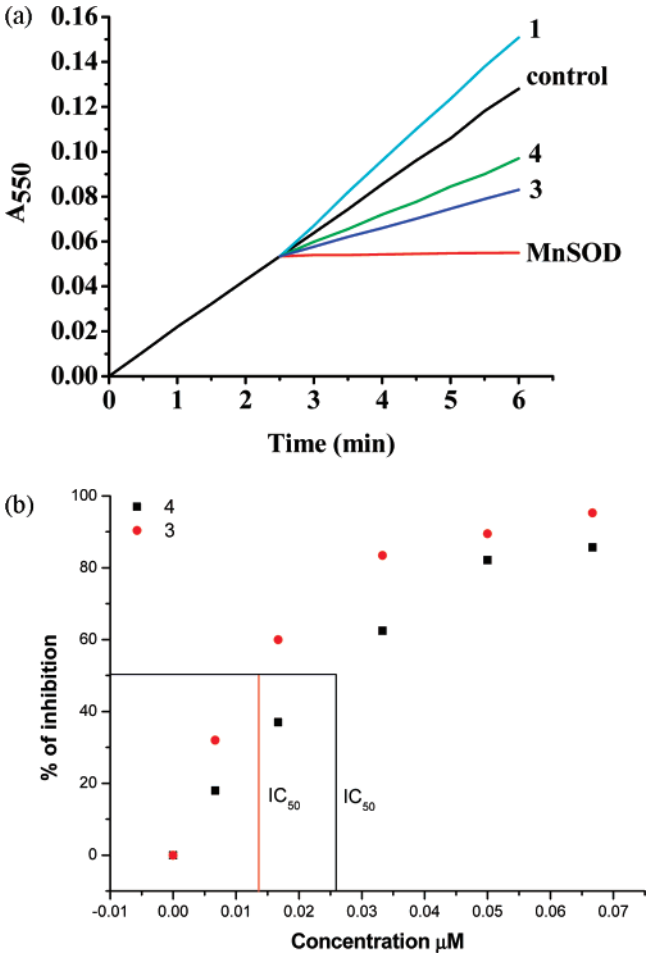

Figure 8. (a) Kinetics of the reduction of ferricytochrome *c* (550 nm) without and with the putative SOD mimics. Reduction of ferricytochrome *c* (followed during 300 s) caused by the addition of the indicated concentrations of tested complexes and MnSOD (*E. coli*). (b) Inhibition percentage as a function of the concentrations of **4** and **5**: IC_{50} determination.

We also have observed that the catalytic rate constants obtained by using a X/XO assay (Table 3) are at least 1 order of magnitude higher than those obtained by a stopped-flow method. We found this to be due to the direct reaction between complexes and cytochrome *c*. When higher complex concentrations than those that cause nearly 100% inhibition were used, a reoxidation of reduced cytochrome *c* was observed, suggesting that the oxidized form of the complex (generated during the catalytic cycle) acts as an oxidant of cytochrome *c*.[31]

The iron complex exhibits an opposite effect, acting in its reduced form as a reductant of cytochrome c, and increases

(29) Butler, J.; Koppenol, W. H.; Margoliash, E. *J. Biol. Chem.* **1982**, *257*, 10747−10750.

(30) (a) Liao, Z.-R.; Zheng, X.-F.; Luo, B.-S.; Shen, L.-R.; Li, D.-F.; Liu, H.-L.; Zhao, W. *Polyhedron* **2001**, *20*, 2813−2821. (b) Rodriguez, M.-C.; Morgenstern-Badarau, I.; Cesario, M.; Guilhem, J.; Keita, B.; Nadjo, L. *Inorg. Chem.* **1996**, *35*, 7804−7810. (c) Gauuan, P. J. F.; Trova, M. P.; Gregor-Boros, L.; Bocckino, S. B.; Crapo, J. D.; Day, B. J. *Bioorg. Med. Chem.* **2002**, 3013−3021. (d) Kitajima, N.; Osawa, M.; Tamura, N.; Morooka, Y.; Hirano, T.; Hirobe, M.; Nagano, T. *Inorg. Chem.* **1993**, *32*, 1879−1880. (e) Xiang, D. F.; Tan, X. S.; Hang, Q. W.; Tang, W. X.; Wu, B.-M.; Mak, T. C. W. *Inorg. Chim. Acta* **1998**, *277*, 21−25. (f) Spasojevic, I.; Batinic-Haberle, I.; Stevens, R. D.; Hambright, P.; Thorpe, A. N.; Grodkowski, J.; Neta, P.; Fridovich, I. *Inorg. Chem.* **2001**, *40*, 726−739. (g) Kachadourian, R.; Batinic-Haberle, I.; Fridovich, I. *Inorg. Chem.* **1999**, *38*, 391−396.

(31) Detailed kinetic investigations are in progress.

the slope of cytochrome *c* reduction when injected into solution (Figure 8a).[31] Thus, the calculation of its IC_{50} and *k*McCF were not possible. To prove its activity in aqueous medium, we used a modified NBT assay. Here, instead of xhanthine/xhantine oxidase system, KO_2 was used as source of superoxide. When **1** was present in solution, an inhibition of blue formazan formation was observed in a concentration dependent manner. The concentration of **1** that caused 50% inhibition of formazan formation (followed at 580 nm) was 6.45 μM. **4** caused 50% inhibition at the concentration of 1.36 μM, while **3** showed no effect. However, we observed that **3** reacts with NBT itself, presumably forming a new complex that, if the higher complex concentrations ($>1 \times 10^{-3}$ M) were used, immediately precipitated as a yellow powder. The solution of **1** ($>1 \times 10^{-3}$ M) gets slightly milky in the presence of NBT after 1 day, whereas no interaction between **4** and NBT was observed. Interactions with the NBT indicator account for no detectable SOD activity of **3** and somewhat lower activity of **1** than would be expected based on the stopped-flow measurements.

Although neither of the indirect methods we used proved to be reliable, they show, in the manner utilized in the literature,[6,18,30] that our complexes exhibit substantial SOD activity in aqueous solutions as well.

Conclusions

Although it has been postulated in the literature that only seven-coordinate complexes of macrocyclic ligands with prominent conformational flexibility could possess SOD activity,[8g,32] our seven-coordinate iron and manganese complexes with the acyclic and rigid H_2dapsox ligand demonstrate the ability for catalytic decomposition of superoxide. Similar to what usually was found in the case of the macrocyclic pentadentate ligands,[11] the manganese complex shows higher SOD activity than the corresponding iron complex. However, higher stability of the iron complex over a very wide pH range is an advantage in terms of a possible application.

The demonstrated SOD activity of the rigid seven-coordinate complexes is in agreement with our recent findings that water release and formation of a six-coordinate intermediate, requiring conformational rearrangement of the ligand, is not the rate-limiting step in the overall inner-sphere catalytic SOD pathway of the proven macrocyclic SOD mimetics.[12a] Furthermore, it also shows that conformational flexibility of the pentadentate ligand is not the key factor assisting SOD activity and that the acyclic and rigid ligand systems can also be considered as structural motifs for the design of SOD mimetics. An additional advantage can be the fact that their syntheses are more economic than the syntheses of macrocyclic ligands.

We have also shown that the indirect SOD assays, which are the most used methods for demonstrating complex SOD activity, are not very reliable[10] and can be applied only upon considering possible cross-reactions between the indicator substance and the studied complex in their different oxidation forms, in which they may occur within the SOD catalytic cycle. The direct stopped-flow method, where a high excess of superoxide over the complex can be utilized, is a better probe for a complex SOD activity even though it requires a DMSO medium. Importantly, as was stressed by Sawyer et al., an even closer relation between the kinetic measurements in aprotic media than in bulk water can be drawn with the processes in mitochondria, which are the major source of superoxide in the aerobic organisms, because aprotic media "may be representative of a hydrophobic biological matrix".[33] Under less protic conditions, causing a longer half-life of $O_2^{\bullet -}$, efficient superoxide decomposition is even more desirable.

Acknowledgment. The authors gratefully acknowledge financial support from the Deutsche Forschungsgemeinschaft within SFB 583 "Redox-active Metal Complexes". We are also thankful to Prof. R. van Eldik for helpful discussions.

Supporting Information Available: X-ray crystallographic files in CIF format for the structure determinations of complexes **2**−**4**, a table listing the analysis of hydrogen bonds for the crystal structures of **2** and **3**, and cyclic voltammogramms for **1** (variable concentrations) in DMSO purged with dioxygen, for **3** and **4** in an aqueous solution, and for **4** in DMSO purged with dioxygen. This material is available free of charge via the Internet at http://pubs.acs.org.

IC7012039

(32) Riley, D. P. *Adv. Inorg. Chem.* **2007**, *59*, 233−263.

(33) Chin, D.-H.; Chiericato, G., Jr.; Nanni, E. J., Jr.; Sawyer, D. T. *J. Am. Chem. Soc.* **1982**, *104*, 1296−1299.